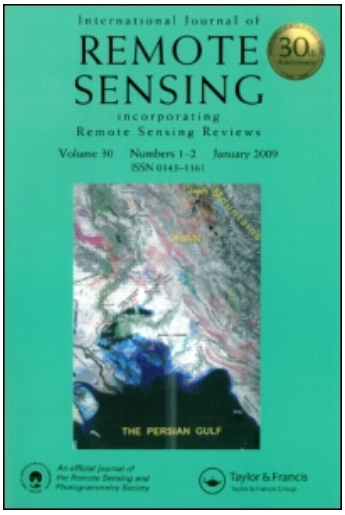

International Journal of Remote Sensing
Publication details, including instructions for authors and subscription information:
http://www.informaworld.com/smpp/title~content=t713722504

Modelling scanning and staring imaging infrared sensors using a static performance model

C. Salvaggio[ab]; S. Israel[a]; Y. T. Kang[a]; M. L. Bartholomew[a]; D. M. Pokrzywka[a]; J. S. Davis[c]; M. J. Duggin[a]
[a] College of Environmental Science and Forestry, State University of New York, Syracuse, New York, U.S.A [b] Digital Imaging and Remote Sensing Laboratory, Center for Imaging Science, Rochester Institute of Technology, Rochester, New York, U.S.A [c] Ball Aerospace Systems Group, Systems Engineering Division, Albuquerque, New Mexico, U.S.A

To cite this Article Salvaggio, C. , Israel, S. , Kang, Y. T. , Bartholomew, M. L. , Pokrzywka, D. M. , Davis, J. S. and Duggin, M. J.(1990) 'Modelling scanning and staring imaging infrared sensors using a static performance model', International Journal of Remote Sensing, 11: 12, 2311 — 2328
To link to this Article: DOI: 10.1080/01431169008955177
URL: http://dx.doi.org/10.1080/01431169008955177

INT. J. REMOTE SENSING, 1990, VOL. 11, NO. 12, 2311–2328

Modelling scanning and staring imaging infrared sensors using a static performance model

C. SALVAGGIO†‡, S. ISRAEL†, Y. T. KANG†,
M. L. BARTHOLOMEW†, D. M. POKRZYWKA†,
J. S. DAVIS§ and M. J. DUGGIN†

† College of Environmental Science and Forestry, State University of New York, 308 Bray Hall, Syracuse, New York 13210, U.S.A.
‡ Digital Imaging and Remote Sensing Laboratory, Center for Imaging Science, Rochester Institute of Technology, One Lomb Memorial Drive, Rochester, New York 14623, U.S.A.
§ Ball Aerospace Systems Group, Systems Engineering Division, 2901 Juan Tabo, N.E., Suite 235, Albuquerque, New Mexico 87112, U.S.A.

(Received 12 May 1989; in final form 11 October 1989)

Abstract. The introduction of mathematical modelling concepts to assess sensor performance is a necessary part of the graduate curriculum in remote sensing science. In this way, the concepts of sensor design and performance assessment under various imaging conditions can be best understood. In this paper, a graduate class project is described in which a static performance model was used to predict the minimum detectable temperature performance, the minimum resolvable temperature performance and the recognition performance of scanning and staring focal plane array (FPA) infrared imaging sensors with three different detector materials. Different seasonal, atmospheric, cold shield angle, target-to-background temperature contrast, bandpass and noise parameters were considered. Such studies are highly labour-intensive and (as in this case) may involve several hundred modelling runs. However, such projects provide a 'real world' experience for those who will design, use and analyse the data from imaging sensors. We present this paper as an approach to providing an in-depth understanding of sensor design concepts and limitations.

1. Introduction

The analysis of image forming systems has been studied by many workers. Some have been interested in the number of line pairs/mm necessary to discriminate military targets from background for given signal-to-clutter (SCR) ratios (e.g. Weathersby and Schmieder 1984). Analytical studies have been performed by several groups. The work of Johnson (1958) was useful but dealt with image intensifiers. This work was extended by Ratches (1976) in developing the Night Vision Laboratories Static Performance Model (NVLSPM) for thermal imaging systems. The NVLSPM is for thermal imaging devices where performance is defined for static (non-time varying) parameters controlling detection, recognition and identification for a given system, atmosphere and target as a function of range. The target, atmosphere, device and observer behaviour are described by equations which result in prediction of system noise equivalent temperature difference (NEΔT), minimum resolvable temperature difference (MRT) and minimum detectable temperature difference (MDT). Detection and recognition are then based on these quantities through algorithms using the required signal-to-noise ratio (SNR) and empirical resolution criteria. The NVLSPM does not, however,

consider focal plane array (FPA) charged-coupled devices (CCD) in the form proposed by Ratches *et al.* (1975) and Ratches (1976). It is designed for night vision devices, first generation FLIRs, etc. The NVLSPM output assumes a TV monitor, viewed in real-time by an operator.

Discussion of models used to specify similar types of thermal imagers is set out in a guide to preparing specifications for thermal imaging systems by a tri-service working group under the sponsorship of the Joint Technical Coordinating Group-Thermal Imaging Systems (JTCG-TIS). This is reported by Wood *et al.* (1976). Overington (1976, 1982) has done a great deal of work on the psychophysiology and neurophysiology of human vision. He has put together a set of widely applicable conceptual models of photopic visual performance. This suite of models is called ORACLE and the model has been implemented not only on mainframe computers, but also on desk-tops (Overington and Greenway 1987). Performance estimates have been considered theoretically (Emmons 1977, Jamieson 1976). Studies have been reported of optimization of the spectral (electromagnetic wavelength) bandpasses and peak wavelengths for infrared system optimum performance (Eldering 1964, Longshore *et al.* 1976). Considerations have been given to optimizing images obtained from sensing devices. For example, Fried (1981) and Fried and Williams (1977) have considered means of correcting a sequence of images in order to enhance a target which may be moving, using a method known as pseudoregistration. Fried and Williams (1977) have considered clutter leakage approximations for staring mosaic sensors with simultaneous line-of-sight (LOS) drift and jitter. Such approximations are taken to apply when LOS motion is a fraction of a pixel-per-frame time. These concepts have also been pursued by Barry and Klop (1982) and Patterson *et al.* (1986). Overington and Greenway (1987) discuss a method of edge detection, based upon the human eye, which is capable of enabling sub-pixel (i.e. sub-resolution) detection accuracy, where the receptors are hexagonal in shape of the focal plane.

Borg *et al.* (1986) describe an updated version of the Night Vision Laboratories NVLSPM. The updated version was written for the US Army Missile Command (MICOM) and is called MI2SPM (MICOM Infrared Imaging Systems Performance Model). We shall concentrate here upon the sensor model, since this model has been developed for FPAs as well as scanning sensors.

The sensor model must account for sensitivity and resolution of the system. Sensitivity is related to noise. Sensor noise can be quantified by noise equivalent power (NEP) and NEΔT from mean background. The preferred measure is NEΔT. NEΔT and the modulation transfer function (MTF) combine to determine the MDT or the MRT. The MDT or MRT equations are used to represent the thermal imaging system, depending upon whether the situation involves a resolved target image, allowing the operator to recognize target features amidst background clutter (where MRT is the criterion) or whether the detection of an unresolved hot spot against a uniform background is required, in which case MDT is the criterion. The MDT and MRT calculations in the MI2SPM follow the same principles as in the NVLSPM. For FPAs, the user can specify the cold shield angle, quantum efficiency and detector mode (photovoltaic or photoconductive) at the keyboard. The code calculates an ideal $D^*(T, f)$ and scales it for cold shield angle, quantum efficiency and the detector mode.

In this paper, we describe a graduate class experiment in which the MI2SPM code was used to compare scanning and staring sensors with different detector materials. We shall describe the model according to the major modules into which the code is divided. Modelling studies of this kind involve several hundred model runs and provide an

excellent opportunity for advanced-level graduate students in remote sensing to obtain in-depth understanding of the factors controlling sensor design and performance.

2. Use of the MI2SPM

The target module allows the user to specify a scene consisting of a simple rectangular target of uniform temperature with an average difference in temperature from a constant temperature background. The radiance from this scene is then propagated along a horizontal path through an assumed homogeneous atmosphere. The atmosphere is defined according to the major aerosol composition (size and distribution) by three specified atmospheric input values; air temperature, relative humidity, and visibility. Here the absorbing atmosphere is defined by the temperature and relative humidity and the scattering atmosphere by the visibility, a function primarily of aerosol number density. A scattering and absorbing transmittance parameter are separately computed for the defined atmosphere and the total atmospheric transmittance is determined as the product of these separate components. The baseline atmospheric model used for these predictions is TABLOW – a modified version of the Air Force Geophysics Laboratories LOWTRAN 6 transmittance/path radiance code. The NVLSPM operates along a horizontal path, which eliminates some inaccuracies inherent in the layering concept present in the LOWTRAN 6 code. It should be noted that LOWTRAN 6 and therefore TABLOW are single scattering models. This infers that as energy is scattered from the beam between the target and the sensor, energy is lost. No energy is allowed to be scattered back into the beam from adjacent energy paths. However, empirical approximations within TABLOW do provide improvement over LOWTRAN 6 in the calculation of path radiance. Furthermore, no time-dependent variations in atmospheric transmission, target-to-background radiance values or dispositions are considered. For this reason, the model is referred to as a static performance model.

Once the contrast has been attenuated by the atmosphere by source attenuation and by the addition of path radiance, the model predicts the transfer and noise characteristics of the sensing system under consideration. The current version of the MI2SPM code will allow either a conventional scanning sensor or an FPA CCD to be simulated. The model predicts transfer characteristics according to an evaluation of the MTF functions of the following system components; atmosphere, line-of-site jitter, optics, detector, system electronics, display, and/or the observer's eye. These components are accounted for when the sensing system is either a scanner or a FPA CCD. In addition to these individual MTFs mentioned, in the case of a FPA CCD the following component MTFs are also included; FPA discrete sampling, charge transfer efficiency, over-exposure, and image reconstruction. These components are cascaded together for each spatial frequency according to

$$MTF_{system} = MTF_{atmo} * MTF_{l.o.s.} * MTF_{optics} * \ldots * MTF_{eye}$$

This cascaded MTF function is used to define the effect of radiometric contrast transfer efficiency through the specified system for each spatial frequency.

The noise characteristics of the sensing system are defined by the NEΔT of the detector. NEΔT is defined as the peak root-mean-squared (r.m.s) noise for a particular electronic bandpass. This noise is due to excitation of electrons into the conduction band of the semiconductor used for the detector due to thermal induced vibrations at the molecular level. A noise power spectrum for the particular detector material can also be defined as a function of frequency. The limiting noise for a sensing system can

be specified as detector noise, shot noise or white noise. This choice will be made as a function of the material from which the detector is made and the conditions of the engagement being analysed.

Sensor parameters such as focal length, f-number, optical transmission, blur circle diameter, instantaneous field-of-view (IFOV) in both the x- and y-directions for individual detectors as well as the entire array (for linear arrays and FPAs), array size, peak detectivity ($D^*(T,f)$), spectral distribution of $D^*(T,f)$, cold shield angle, frame rate, overscan ratio and scan efficiency need to be defined for a scanning system. In the case of an FPA, the last three parameters above can be excluded and the following must be defined; IFOV of the array in the x- and y-directions, x and y image reconstruction filter frequencies to allow a continuous image to be reconstructed from the sampled image, single detector charge transfer efficiency, the number of transfer gates, and the detector readout time. These sensor parameters allow the model to predict the signal level produced for a static, staring system. A wide range of detector materials can be modelled provided that all the necessary detector specific parameters are definable.

Once the energy transfer is completed from the target through the atmosphere and sensor, the model will predict the minimum detectable temperature and minimum resolvable temperature as a function of target size and spatial frequency, respectively. MDT for a system is defined as the minimum temperature difference that is necessary for an observer (or electronic device) to be able to perceive a thermal target against its background: different size square or round targets have different associated MDT values. This quantity represents the threshold detection capability of a system. MRT is defined as the minimum difference in temperature needed to resolve a standard 4-bar target with a 7:1 aspect ratio oriented perpendicular to the scan line or to either axis of an FPA CCD.

We shall first consider the detection situation where the target is distant, but hot, such as an aircraft against a sky background. Here we use MDT as the detection criterion. The signal-to-noise ratio is calculated using the MDT equation and varies with the range of the target. The relationship between the signal-to-noise ratio and the probability of detection is obtained from empirical data, such as that of Rosell and Wilson (1974). A relationship between range and probability of detection is then calculated for 'hot-spot' detection, in which the target is hot enough to make one IFOV different from the background. Under these conditions, detection is a function of signal-to-noise ratio and not the sensor's ground resolution.

A second situation is also considered, where the observer needs a small amount of resolution to see edges or internal features to distinguish the target from background clutter. Here, MRT is the criterion for target detection used to calculate the signal-to-noise ratio. The range is determined for various levels of probability of detection in the same manner as for the case of 'hot-spot' detection.

Recognition is a higher-order discrimination problem: it is defined as the ability to identify specific objects in a class of similar objects. The difficulty encountered in recognition varies with the level of detail needed to make the above identifications. The M12SPM code uses the Johnson (1958) criteria as a means of measuring recognition performance. A bar pattern is considered, based on the target's critical dimension and difference in temperature from the background. The number of cycles to be resolved across a target's critical dimension are computed and compared with the Johnson criteria, so as to determine recognition probability. The 'critical' dimension is generally taken to be the minimum dimension of a protected image of the target as seen by the observer. Since a 'cycle' corresponds to a resolved dark element and an adjacent bright

element, being able to resolve, for example, six elements across the target's critical dimension (the Johnson criterion for 50 per cent probability of recognition) corresponds to three cycles across the target's critical angular subtense.

Recognition probability varies with range and atmospheric transmission. Transmission effects will reduce the overall scene contrast and therefore reduce the peak-to-peak radiance variations between the bars, as well as reducing their angular separation, therefore reducing the probability of recognition. As with detection performance, recognition performance is calculated using the model in the x-, y- and 45-degree orientation directions of the sensor with the target.

The following section defines the target-sensor scenarios which were modelled for this research. Two midwave infrared detector materials, indium antimonide, InSb (a photodetector) and plantinum silicide, PtSi (a Schottky-barrier diode), were used along with a thermal infrared detector material, mercury–cadmium–teluride, HgCdTe. The relative performance of these detector materials in scanning and staring (FPA) sensors will be presented and compared in the results section.

3. Experimental approach

Evaluations were to be made of three detector materials; InSb and PtSi in the midwave infrared (MWIR, 3·5–4·3 μm) and HgCdTe in the longwave infrared (LWIR, 10·0–12·5 μm). These detector materials were used in the following sensor configurations; InSb in a scanner with a 16 element bank of detectors oriented perpendicular to the scan direction and also as a 128×128 element staring FPA; PtSi as a staring 128×128 element FPA; and HgCdTe as both a scanner with a 16-element bank of detectors oriented perpendicular to the scan direction and as a staring 128×128 element FPA. Each of the five sensor configurations were presented with an identical series of imaging scenarios and their detection and recognition performances evaluated and compared. The imaging scenarios included a range of values for the following parameters; season, aerosol composition, target-to-background temperature difference, NEΔT for the particular sensor, cold shield angle and sensor bandpass.

The input deck for each run contains numerous card images for the PC-based version of the MI2SPM used here (Davis, personal communication, 1988). All input decks used in this study are available from the authors upon request. Each input card image begins with a four-letter descriptor indicating the type of information defined. Following the four-letter descriptor, the rest of the card is divided into a number of fields. Each field specifies an input parameter for the program. The input deck is not limited to one run: many different scenarios can be placed in a batch mode without interactive user interface. The program contains default values for most input deck parameters. The default values can be accepted if the user has no information referring to the particular sensor/detector combination being modelled (these default values correspond to a HgCdTe detector). 'Typical' detector data was obtained from the literature and from Borg (personal communication, 1988).

For each of the three detectors and sensor types, the target size, background temperature, visibility and the latitude of imaging were held constant. The independent variables were season, aerosol composition, target-to-background temperature difference, NEΔT, cold shield angle, and bandpass in terms of a lower and upper wavelength. Range was computed for a 95 per cent or greater probability of detection or recognition (conservative and optimistic cases were both considered).

The target simulated a T-65 tank viewed from the side; approximated by a 6·5 by 2·5 m rectangular target of constant temperature. The background temperature was set

at 20°C. The imaging occurred in a mid-latitude environment with a visibility of 13 km. The seasonal variation was limited to summer and winter conditions while the aerosol composition was limited to either rural or urban. The seasonal and aerosol values are input parameters for TABLOW which computes environmental specifications based on a collection of empirical data. The target-to-background temperature difference allowed the probability of a target being distinguishable from its background to be observed. The observed radiance at the sensor for a target and its background depends upon the average temperature field present in the ground resolution cell. The values for target-to-background temperature difference were set at 2·5°C, 5°C, 10°C, and 15°C. Cold shield angle was taken to be 30° or the minimum angle subtended by the detector array for each sensing system. Only one bandpass was modelled in the thermal infrared region, 10·0 to 12·5 μm. In the MWIR region, the radiation observed by a sensor is both reflected and emitted. The 3·5 to 4·3 μm bandpass was treated as a whole as well as two sub-intervals, 3·5 to 3·9 μm and 3·9 to 4·3 μm. The band separation was carried out in order to evaluate split band performance differences.

The comparison of the effects of each independent variable was carried out as follows. For each sensing system, the mean of the four dependent range variables mentioned previously was computed as a function of each of the independent imaging parameters, season, aerosol, etc., for each bandpass. The difference in these mean values for each dependent variable was checked for statistical significance at a confidence level of 0·05. For the case where the independent variable took on only two values, a two-sample student's t-test was used while for cases where the independent variables took on three or more levels, a two-way analysis of variance was employed. These results are presented graphically in the following section.

4. Results

The MI2SPM infrared modelling code was executed under a number of different imaging conditions. Three detector materials; InSb, PtSi and HgCdTe were each modelled in a 128×128 element staring FPA sensor. InSb and HgCdTe were also modelled in a scanning device.

In order to perform a comparison of the detector materials and sensing configurations, six independent variables were modified in a systematic process. These independent variables included target-to-background temperature difference (ΔT), NEΔT, season, aerosol composition, cold shield angle and bandpass (in the case of the InSb and PtSi detector materials). The effect of these six parameters was observed on four dependent variables. These quantities were the maximum ranges allowable to maintain a 95 per cent confidence level of the near field-of-view MRT, and MDT and both conservative and optimistic recognition performance.

The manner in which this data was analysed involved determination of the mean of each of the dependent variables (ranges) as a function of the discrete values of the independent variables. For example, the mean values for the four range variables was found while the season variable was set as summer and also as winter. The averaging involved many different values of range for which there was a number of different combinations of the remaining five independent values. This will tend to indicate what effect, if any, the parameter held constant presented to these range variables. In the case where the independent variable was bi-valued, a two-sample student's t-test was used to test for equality of the mean values at a confidence level of 0·95 ($\alpha = 0{\cdot}05$). In the cases where the independent variable took on more than two values (e.g. for ΔT and bandpass), a two-way analysis of variance (ANOVA) was used to test if all the means

were equal (note that failure of this test means that at least one mean value was not equal). The resulting means and statistical test results appear in the table. It should be noticed that the column labelled *t*-test states the results of either the *t*-test or two-way ANOVA, whichever was applicable for the particular independent variable. An '=' sign indicates that no significant difference due to the independent variable existed at a 90 per cent confidence level while a '≠' sign indicates that the variable did have a significant effect.

Summary of range data obtained at 95 per cent probability of detection/recognition for the following scenario parameters.

		Range (km) for detection/recognition at 95 per cent probability							
		MRT	*t*-test	MDT	*t*-test	Recog. conserv.	*t*-test	Recog. optim.	*t*-test
Season									
InSb FPA	Summer	6·568	=	4·821	=	1·743	=	2·302	=
	Winter	6·669		4·823		1·745		2·302	
InSb SCA	Summer	7·393	=	4·851	=	1·870	=	2·550	=
	Winter	7·406		4·852		1·870		2·550	
PtSi FPA	Summer	6·117	=	4·826	=	1·700	=	2·231	=
	Winter	6·250		4·827		1·708		2·245	
HgCdTe FPA	Summer	2·988	≠	4·829	≠	1·050	=	1·316	=
	Winter	3·592		4·785		1·090		1·407	
HgCdTe SCA	Summer	2·779	≠	4·847	=	0·720	=	0·940	=
	Winter	2·828		4·855		0·720		0·940	
Aerosol									
InSb FPA	Urban	6·604	=	4·824	=	1·744	=	2·302	=
	Rural	6·633		4·821		1·744		2·302	
InSb SCA	Urban	7·393	=	4·850	=	1·870	=	2·550	=
	Rural	7·406		4·854		1·870		2·550	
PtSi FPA	Urban	6·174	=	4·826	=	1·704	=	2·236	=
	Rural	6·194		4·826		1·704		2·240	
HgCdTe FPA	Urban	3·276	=	4·808	=	1·070	=	1·362	=
	Rural	3·304		4·807		1·070		1·362	
HgCdTe SCA	Urban	2·803	=	4·850	=	0·720	=	0·940	=
	Rural	2·803		4·852		0·720		0·940	
Bandpass									
InSb FPA	3·5–3·9 μm	6·790		4·822		1·754		2·326	
	3·9–4·3 μm	6·424	≠	4·819	=	1·732	≠	2·278	≠
	3·5–4·3 μm	6·642		4·825		1·745		2·303	
InSb SCA	3·5–3·9 μm	7·418		4·849		1·870		2·550	
	3·9–4·3 μm	7·381	≠	4·854	=	1·870	=	2·250	=
	3·5–4·3 μm	?		?		?		?	
PtSi FPA	3·5–3·9 μm	6·382		4·827		1·723		2·265	
	3·9–4·3 μm	5·948	≠	4·824	=	1·684	≠	2·208	≠
	3·5–4·3 μm	6·223		4·828		1·704		2·243	
HgCdTe FPA	10–12·5 μm	3·290		4·807		1·070		1·362	
HgCdTe SCA	10–12·5 μm	2·803		4·851		0·720		0·940	

=, no significant difference at the 95 per cent confidence level.
≠, significant difference at the 95 per cent confidence level.

(table cont.)

		Range (km) for detection/recognition at 95 per cent probability							
		MRT	*t*-test	MDT	*t*-test	Recog. conserv.	*t*-test	Recog. optim.	*t*-test
Cold shield angle									
InSb FPA	0·7°	6·619	=	4·822	=	1·744	=	2·302	=
	30°	6·619		4·822		1·744		2·302	
InSb SCA	0·1°	7·430	=	4·853	=	1·870	=	2·550	=
	30°	7·389		4·851		1·870		2·550	
PtSi FPA	0·7°	6·184	=	4·826	=	1·704	=	2·238	=
	30°	6·184		4·826		1·704		2·238	
HgCdTe FPA	2·4°	3·290	=	4·807	=	1·070	=	1·362	=
	30°	3·290		4·807		1·070		1·362	
HgCdTe SCA	0·7°	2·803	=	4·851	=	0·720	=	0·940	=
	30°	2·803		4·851		0·720		0·940	
NEΔT									
InSb FPA	0·05°C	7·035	≠	4·844	≠	1·770	≠	2·350	≠
	0·15°C	6·202		4·800		1·718		2·254	
InSb SCA	0·05°C	7·430	≠	4·853	=	1·870	=	2·550	=
	0·15°C	7·369		4·851		1·870		2·550	
PtSi FPA	0·05°C	6·682	≠	4·846	≠	1·758	≠	2·317	≠
	0·15°C	5·686		4·806		1·650		2·160	
HgCdTe FPA	0·05°C	3·704	≠	4·824	≠	1·170	≠	1·505	≠
	0·15°C	2·876		4·790		0·970		1·219	
HgCdTe SCA	0·05°C	2·828	≠	4·849	=	0·720	=	0·940	=
	0·15°C	2·779		4·853		0·720		0·940	
Target-to-background ΔT									
InSb FPA	2·5°C	5·820		4·792		1·683		2·205	
	5°C	6·462	≠	4·801	≠	1·753	≠	2·303	≠
	10°C	6·999		4·847		1·770		2·350	
	15°C	7·194		4·849		1·770		2·350	
InSb SCA	2·5°C	7·308		4·851		1·870		2·550	
	5°C	7·430	≠	4·853	=	1·870	=	2·550	=
	10°C	7·430		4·851		1·870		2·550	
	15°C	7·430		4·851		1·870		2·550	
PtSi FPA	2·5°C	5·259		4·798		1·584		2·038	
	5°C	5·958	≠	4·815	≠	1·691	≠	2·230	≠
	10°C	6·601		4·848		1·770		2·335	
	15°C	6·918		4·844		1·770		2·350	
HgCdTe FPA	2·5°C	2·494		4·769		0·878		1·098	
	5°C	3·098	≠	4·806	≠	1·015	≠	1·209	≠
	10°C	3·664		4·825		1·158		1·475	
	15°C	3·905		4·829		1·230		1·585	
HgCdTe SCA	2·5°C	2·718		4·849		0·720		0·940	
	5°C	2·815	≠	4·858	=	0·720	=	0·940	=
	10°C	2·840		4·846		0·720		0·940	
	15°C	2·840		4·851		0·720		0·940	

=, no significant difference at the 95 per cent confidence level.
≠, significant difference at the 95 per cent confidence level.

The data was then presented in a graphical format (see the figure). If a significant difference existed between the mean range values obtained for the different levels of the independent variable under question, the data was plotted. Data which presented no significant difference warranted no graphical analysis.

In looking at the graphical representations on the following pages and the table observations can be made as to the effects induced by the independent variables. What follows is a brief collection of observations made for each of the conditions. More general conclusions will be drawn in the following section.

4.1 *Target-to-background ΔT*

Range for MDT changed very little with differing values of ΔT. Since MDT is inherently a binary quantity, either a target is perceived as anomalous against the background or it is not, once there is 95 per cent confidence that an anomaly exists, then an increase in ΔT will not dramatically change the range at which this confidence is achieved.

Range for MRT undergoes quite a dramatic change with ΔT. The reason for this is that the range at which a 4-bar target with 7:1 aspect ratio can be resolved increases as the contrast of the bar target increases. The greater the value of ΔT, the greater the modulation between the bars and the spaces, therefore the range at which the target can be resolved with 95 per cent confidence also increases.

Recognition at 95 per cent confidence undergoes little change with ΔT. At the point where there is a sufficient number of cycles across the target with sufficient contrast to achieve recognition according to the Johnson criteria, an increase in this contrast level will not allow the target to be resolved at greater ranges since it is the number of cycles across the target that is the driving factor for recognition performance. This result indicates that the ΔT parameter defined for this effort is sufficient to allow the sensor to operate near its theoretical resolution limit.

The largest effect induced by a change in this variable was MRT for FPAs. This same effect was relatively small on the scanning geometries. In all cases where a significant difference did exist in the dependent variables, the InSb detector material provided a greater range than the PtSi material.

4.2. *NEΔT*

An increase in NEΔT results from an increase in the noise of the sensor. This increase in noise level provided a significant decrease in the range at which detection or recognition occurred at the 95 per cent probability level for all sensors with the exception of the InSb and HgCdTe scanners. With a scanning system, the noise due to the short integration time (consisted of dark noise, shot noise, etc.) dominates over any differences provided by the 0·1°C change in NEΔT which was simulated in this research. Perhaps a larger change (from 0·05°C to 0·15°C) in NEΔT would provide a significant effect for these scanning systems.

MRT was the most affected by NEΔT of the four range variables. Approximately a 1 km change in range resulted for all the FPA sensors (increased NEΔT resulted in a decreased range at which detection occurred at the 95 per cent probability level). This occurs since the low-level modulation, particularly at high spatial frequencies, becomes masked by the increase in noise.

MDT is less affected by NEΔT since noise superimposed on a uniform target against a uniform background will still result in a difference in the r.m.s. level of the target and background fields. Only when MDT approaches four times the level of

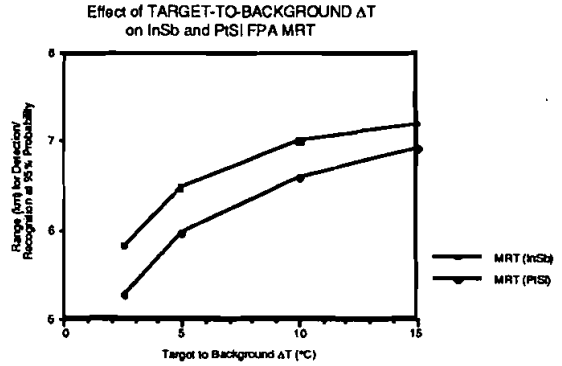

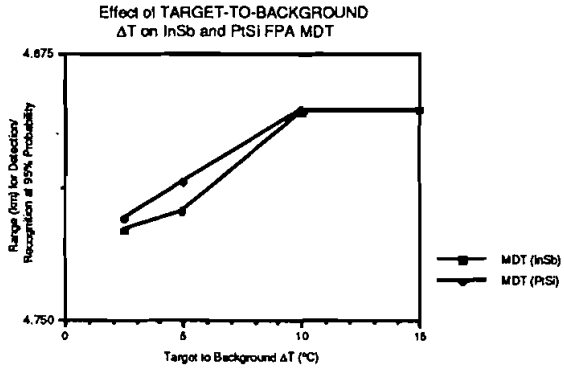

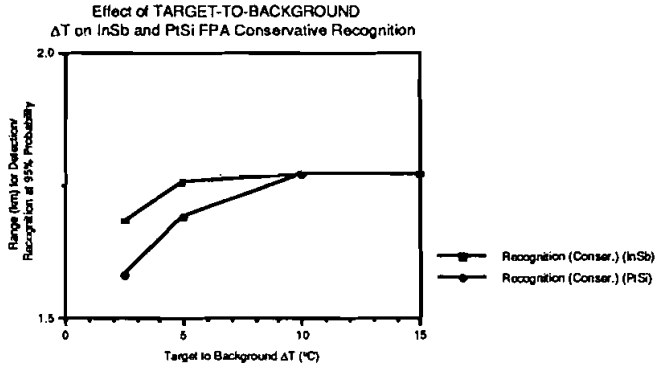

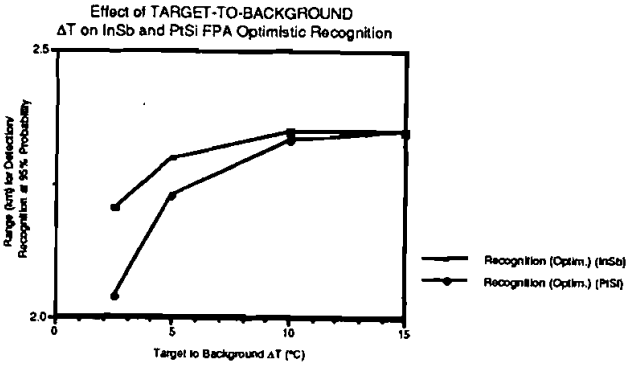

(*a*)

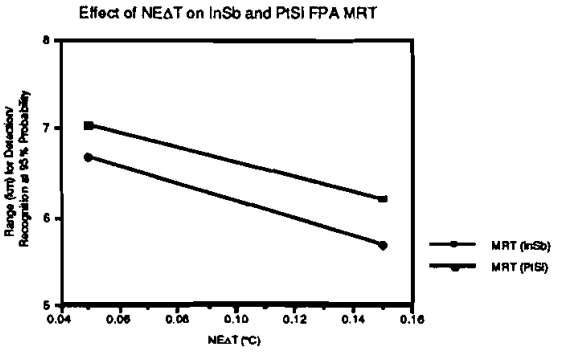

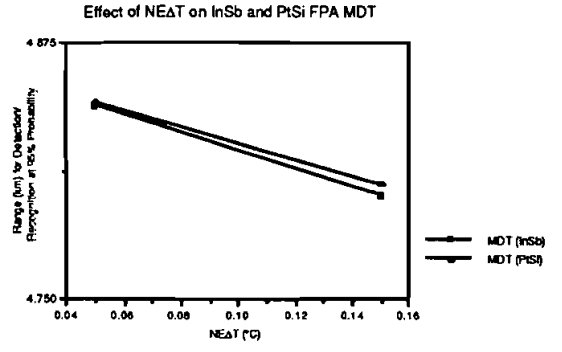

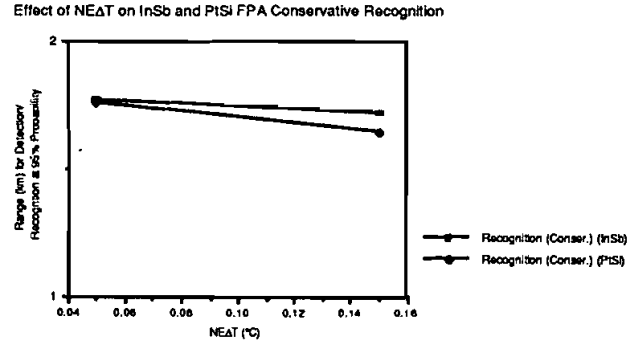

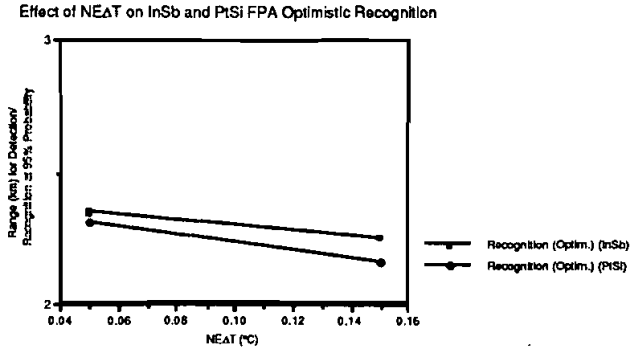

(*b*)

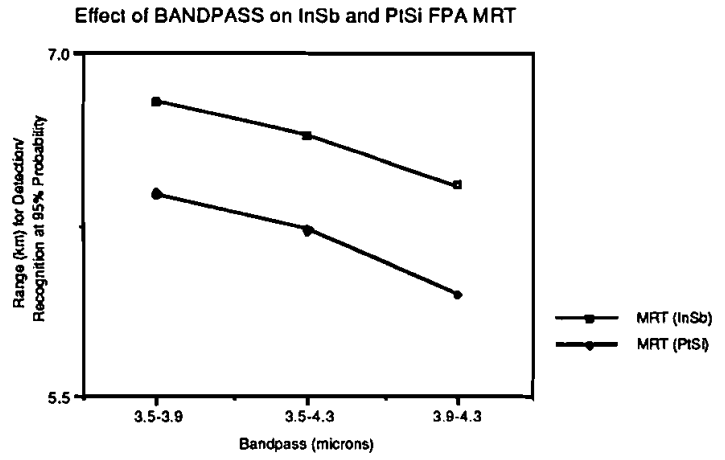

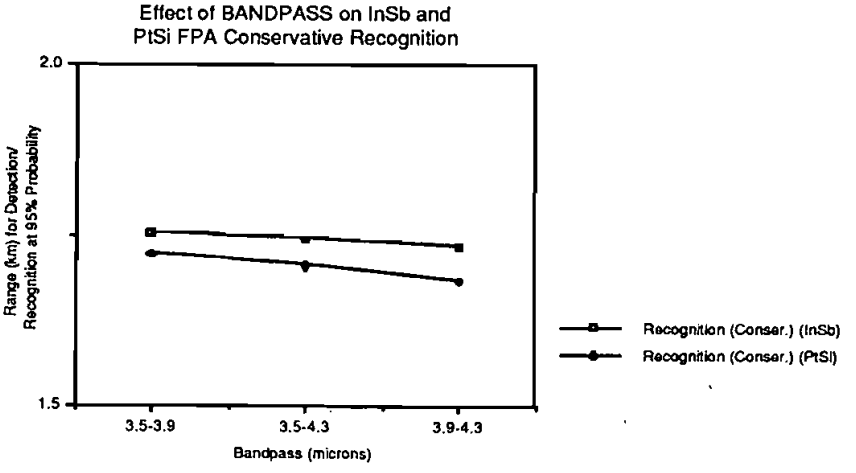

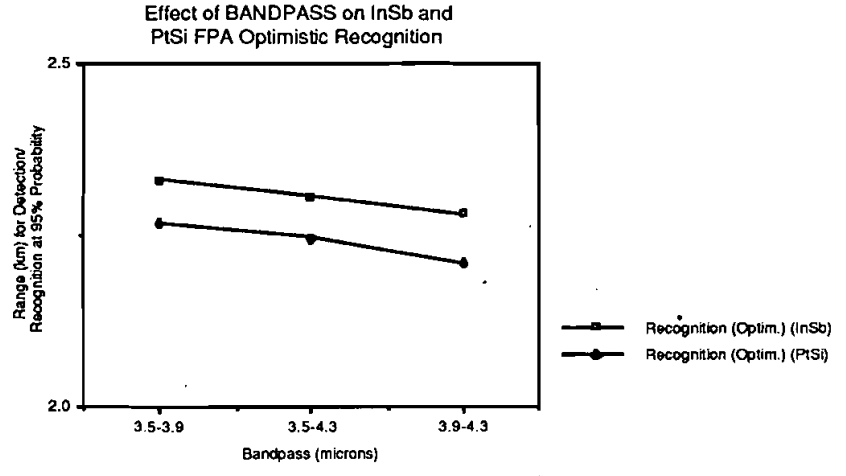

(c)

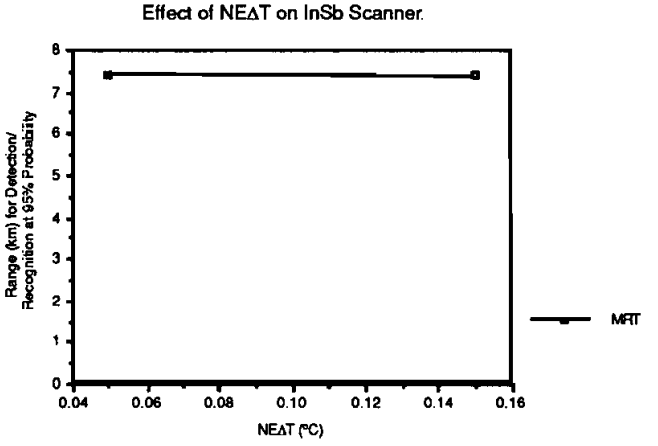

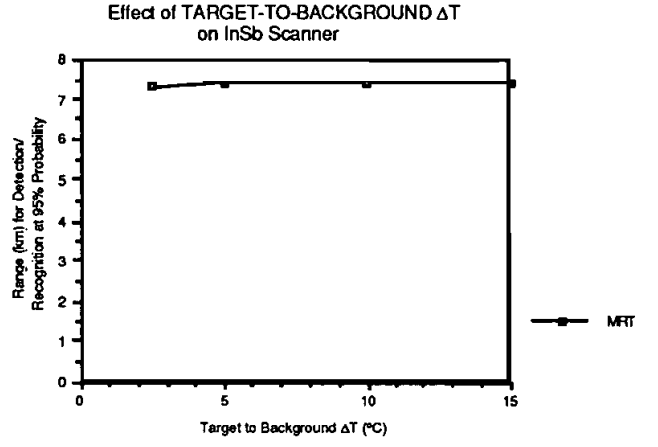

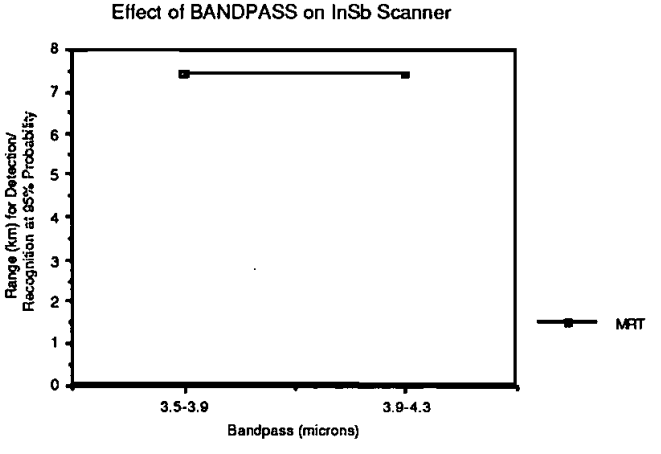

(*d*)

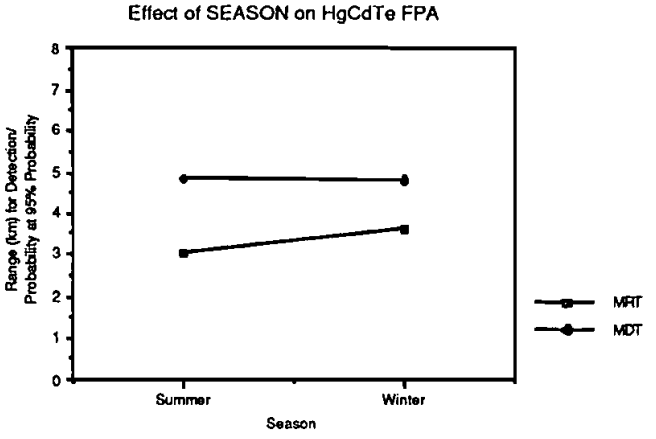

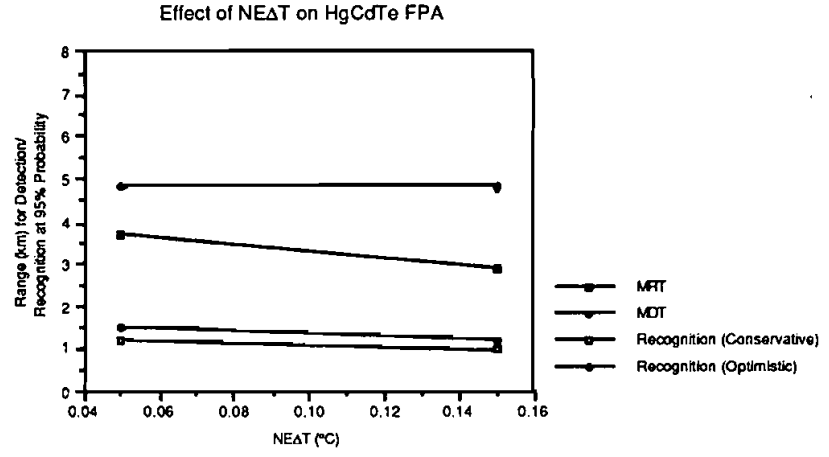

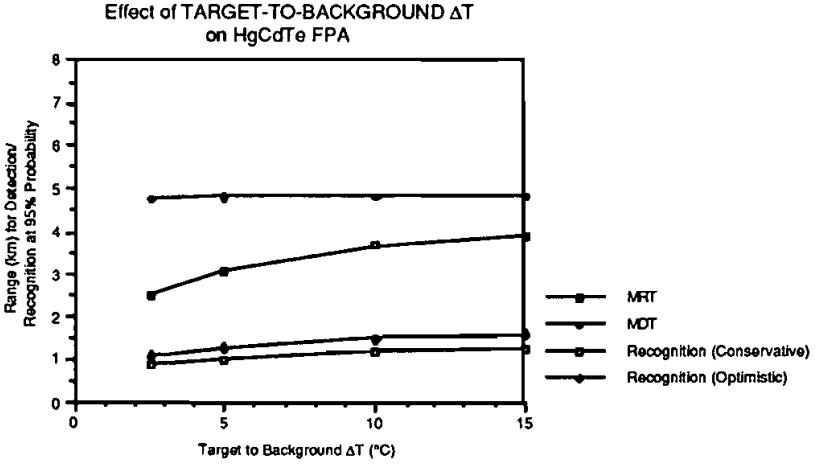

(*e*)

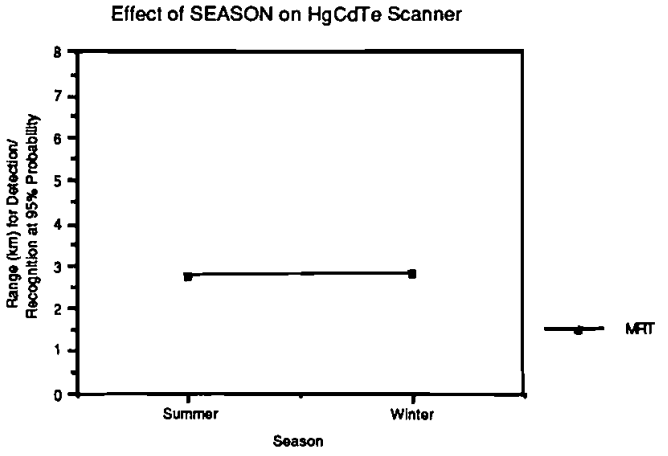

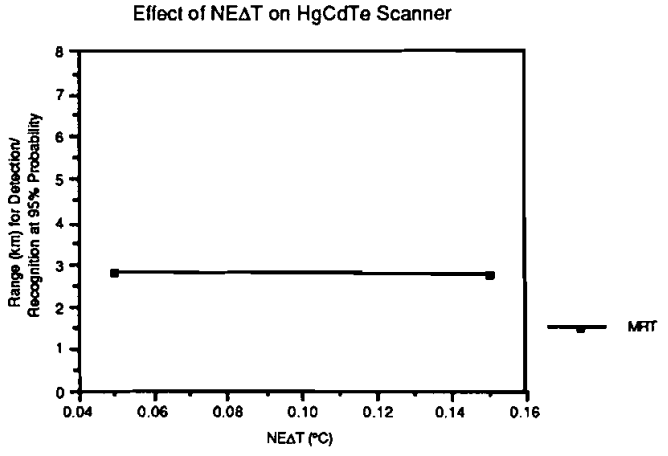

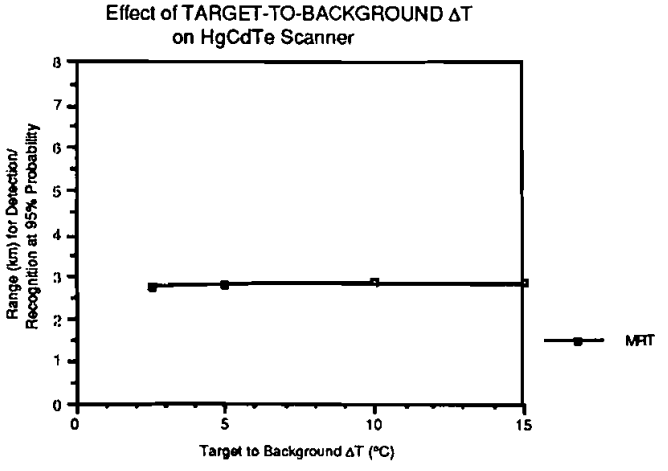

(*f*)

NEΔT will the value of NEΔT become a problem (since a signal-to-noise level of four is the criterion for detection with a 95 per cent probability of being correct).

Recognition is dominated by the spatial distribution of contrast boundaries and therefore a sufficiently low value of NEΔT is required to discriminate these boundaries so as to be able to achieve recognition.

4.3. *Bandpass*

The bandpass was only changed with midwave IR sensors. The bandpass 3·5 to 4·4 μm was used as were two sub-intervals, 3·5 to 3·9 and 3·9 to 4·3 μm. These split bands provided a significant difference in MRT for both conservative and optimistic recognition performance. The reason for this difference was the dramatic change in resolved energy in these two bandpasses. The 3·5 to 3·9 μm bandpass records a higher reflected energy component than the 3·9 to 4·3 μm bandpass. This led to the increase in the range at which detection at the 95 per cent probability occurred for these variables.

The most significant effect resulted in the MRT range for the FPAs. Approximately a 0·5 km difference in the range at which detection could be expected with a 95 per cent probability resulted from the change in bandpass with the 3·5 to 3·9 μm bandpass resulting in the best performance. The 3·5 to 4·3 μm bandpass yielded, as would be expected, results which fell amidst the two sub-divisions of this bandpass.

4.4. *Season*

The effect which resulted from a change in season (winter and summer) on the HgCdTe FPA and scanning sensors was very small (the difference most likely occurring as a result of the cooler winter air contributing less to the path radiance). This seasonal change resulted in a 0·5 km change in range for 95 per cent probability of detection for the FPA while the change observed for the HgCdTe scanning system was an order of magnitude less. Season could have a greater effect if the model included interactions of the surrounding environment with the target and background (i.e. convective cooling, wind effects, etc.).

4.5. *Aerosol*

This independent variable had no effect on the ranges computed. The visibility was held constant throughout this study at 13 km and the relative humidity did not change. Therefore it can be observed that the different aerosol constituents in an urban and rural atmosphere had no effect on the performance of the systems.

4.6. *Cold shield angle*

This variable also had no effect on the ranges determined. The values for cold shield angle which were used consisted of a value which was slightly larger than the acceptance angle of the sensor as well as a value which was significantly larger. Since neither of these angles impinged on the incoming signal, it is not surprising that no effect was observed. With the much larger cold shield angle, one might expect that stray radiation may play a role in affecting the quality of the image, however this was not indicated by our study. In effect, cold shield angle modifies D^* as $D^{*\prime} = (D^*/\sin\zeta)$ where ζ is the cold shield half-angle.

5. Conclusions

The M12SPM model demonstrated a number of factors which must be taken into consideration when dealing with a thermal infrared imaging system. The correlations

between the independent variables and the resulting range data calculated from them for 95 per cent probability of detection and recognition varied between the detector materials, InSb, PtSi, and HgCdTe, and with sensor geometry (FPA or scanner). Although no definitive statement can be made from the test scenarios about all thermal infrared imaging systems, specific observations revealed a number of factors important for consideration.

Of the six independent variables, two of these—aerosol characteristic for the scenarios modelled and cold shield angle—showed little or no effect upon the ranges for 95 per cent detection and recognition probability. However, only urban and rural scenarios were considered; had a marine environment been considered it would be expected that a change would have been seen. Aerosol characteristics for this example are based upon typical mid-latitude urban and rural values. Seasonal variation caused some changes in detection and recognition probability. Both the season and aerosol type are inputs into the transmission model. Since the visibility for all scenarios remained the same, any increase in the amount of aerosols within a given bandpass would not affect the performance. Cold shield angle is the limiting aperture for detector. The simulated scenarios used cold shield angles which were always larger than the acceptance angle of the detector. Since all the detector elements in both cases were fully illuminated, the results did not differ.

Two interesting outcomes are noticed. First, the scanner systems were less sensitive to the changes in the independent variables than the FPA systems. For a scanner using the same material as an FPA no difference in range performance was perceived between these sensors in the *t*-test analysis for detection or for conservative and optimistic target recognition performance. Secondly, the only difference in the results between the conservative and optimistic recognition performance was an increase in range and not a variation among these recognition parameters as determined by the *t*-test analysis.

The seasonal variation affected only the thermal detector, HgCdTe, not the MWIR detectors. Seasonal variation is an input into the transmission model. The winter scenarios resulted in greater ranges for 95 per cent detection and recognition probability in all comparisons. However, in both seasons, background temperature was held constant at 20°C. Since colder air contributes less path radiance and hence has a less degrading effect on contrast, these results are not unreasonable. Therefore, it appears that detection and recognition performance is inversely proportional to air temperature.

The bandpass was divided into two in the MWIR region: the bandpasses considered were 3·5–4·3 μm, 3·5–3·9 μm and 3·9–4·3 μm. It was hypothesized that the different proportions of emitted and reflected radiance in the different bandpass regions could be used as a discriminator. The longer wavelength bandpass (3·9–4·3 μm) exhibited a longer range for 95 per cent confidence in discriminating MDT and MRT, for both conservative and optimistic recognition.

NEΔT affected the performance of FPAs for all detectors, but affected the scanners only in detection performance based upon the MRT criterion. The NEΔT varies inversely with dwell time, detector area and directly with the objective *f*-number. Therefore, as the NEΔT increases, the detection performance will decrease due to the fact that the signal-to-noise ratio will decrease so the target will be less distinguishable from the background.

As for investigations involving changes in NEΔT, the impact on detection and recognition performance of target-to-background temperature difference will be based

on the sensitivity of the system to discriminate an anomaly from noise. The greater the target-to-background temperature, the better the detection performance.

A final, and most important point is that a project of this nature is helpful to graduate students in so far as they gain insight into the entire remote sensing system. This includes an understanding of all those factors modulating the spatial frequencies and electromagnetic wavelength characteristics of the upwelling radiance field, and of the impact of these factors on the detection and recognition performance of an infrared imaging sensor. It is recommended that such studies be included in graduate curriculum for students of remote sensing science.

References

BARRY, P. E., and KLOP, M., 1982, Jitter suppression: A data processing aproach. *Proceedings of the International Society for Optical Engineering (SPIE)*, **366**, 2–9.

BORG, E. J., DAVIS, J. E., and THOMPSON, B. D., 1986, Modeling approaches to thermal imaging systems. *Proceedings of the International Society for Optical Engineering (SPIE)*, **636**, 2–16.

ELDERING, H. G., 1964, The theory of optimum spatial filtering. *Infrared Physics*, **4**, 231–237.

EMMONS, R. B., 1977, Thermal imaging systems performance estimates. *Infrared Physics*, **17**, 415–418.

FRIED, D. L., 1981, Spatial filtering for clutter rejection in (moving) point target detection. *Proceedings of the International Society for Optical Engineering (SPIE)*, **268**, 156–157.

FRIED, D. L., and WILLIAMS, R. D., 1977, Formalism development and sample evaluation of the mean-square background clutter leakage for a HALO type processor. Report No. TR-239. Optical Sciences Company, Los Angeles, California.

JAMIESON, J. A., 1976, Passive infrared sensors: limitations on performance. *Applied Opticis*, **15**, 891–909.

JOHNSON, J., 1958, Analysis of image forming systems. *Proceedings of the Image Intensifier Symposium, Warfare Vision Branch, held in Fort Belvoir, Virginia, on 6–7 October 1958.*

LONGSHORE, R., RAIMONDI, P., and LUMPKIN, M., 1976, Selection of detector peak wavelength for optimum infrared system performance. *Infrared Physics*, **16**, 639–647.

OVERINGTON, I., 1976, *Vision and Acquisition* (London: Pentech Press).

OVERINGTON, I., 1982, Towards a complete model of photopic visual threshold performance. *Optical Engineering*, **21**, 2–13.

OVERINGTON, I., and GREENWAY, P., 1987, Practical first-difference edge detection with sub-pixel accuracy. *Image and Vision Computing*, **5**, 217–224.

PATTERSON, T. J., CHABRIES, D. M., and CHRISTIANSEN, R. W., 1986, Image processing for target detection using data from a staring mosaic infrared sensor in geosynchronous orbit. *Optical Engineering*, **25**, 166–172.

RATCHES, J. A., 1976, Static performance model for thermal imaging systems. *Optical Engineering*, **15**, 525–530.

RATCHES, J. A., LAWSON, W. R., OBERT, L. P., BERGEMANN, R. J., CASSIDY, T. W., and SWENSON, J. M., 1975, Night Vision Laboratory static performance model for thermal viewing systems. US Army Electronic Command, Night Vision Laboratory, Fort Belvoir, Virginia, ECOM-7043.

ROSELL, F. A., and WILSON, R. H., 1974, Performance synthesis of electro-optical sensors. AFAL-TR-74-104, Air Force Avionics Laboratory, Wright Patterson Air Force Base, Ohio.

WEATHERSBY, M. R., and SCHMIEDER, D. E., 1984, An experiment quantifying the effect of clutter on target detection. *Proceedings of the International Society for Optical Engineering (SPIE)*, **510**, 26–33.

WOOD, J. T., BENTZ, W. J., POHLE, T., and HEPFER, K., 1976, Specification of thermal imagers. *Optical Engineering*, **15**, 531–536.